

Highlights of Joint Research

Synchrotron Radiation Laboratory

The 2011 Tohoku Earthquake

On March 11 2011 at 14:46 JST, the 9.0-magnitude undersea megathrust earthquake occurred in the north-western Pacific Ocean and struck the east Japan region with the enormous damage. We have survived from the terrifying disaster without losing any member. We express our deepest sympathies and heartfelt condolences to those who lost family and friends in earthquake and its aftermath.

The earthquake has left large damages at our beamline in Photon Factory and at our office in the Tsukuba branch. Vacuum chambers at the beamline were moved to different positions and some of the components were broken apart. The air leakage and the pump damage were also identified. Almost all the cabinets in the office were fallen down. Members in the laboratory have worked really hard to recover and rebuild the experimental station and the office back again. Thanks to their devoted effort, researches with synchrotron radiation have now been normally made at the beamline since autumn in 2011.

The laboratory activity

The Synchrotron Radiation Laboratory (SRL) was established in 1975 as a research division dedicated to solid state physics using synchrotron radiation (SR). In 1989, SRL started to hold the Tsukuba branch, a branch laboratory in the Photon Factory (PF), High Energy Accelerator Research Organization (KEK). SRL maintains a Revolver undulator, two beamlines and three experimental stations; BL-18A for angle-resolved photoemission spectroscopy with SCIENTA electron analyzer, while undulator beamline BL-19A and BL-19B, for spin- and angle-resolved photoelectron spectroscopy (SARPES) and soft X-ray emission spectroscopy experiments, respectively. They are fully opened to outside users for experiments. The operation time of these beamlines was about 4000 hours and the number of users is more than 100 a year. Recently, a high-yield spin detector, using very low energy electron diffraction, was developed at BL-19A. SARPES measurements have now been performed with high-resolution and the experiments at the beamline have become important to investigate exciting topics of surface/solid state physics such as topological insulators and ferromagnetic nanofilms.

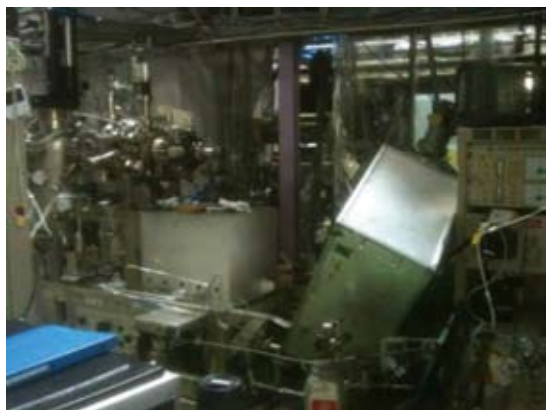


Fig. 1. KEK-PF BL-18A after the earthquake



Fig. 2. Office in the Tsukuba branch after the earthquake



Fig. 3. 3D nano ESCA at Spring-8 BL07LSU



Fig. 4. XES station at Spring-8 BL07LSU

The SRL staffs have joined the Materials Research Division of the Synchrotron Radiation Research Organization (SRRO) of the University of Tokyo and they have played essential role in constructing a new high brilliant soft X-ray beamline, BL07LSU, in SPring-8. The light source is the polarization controlled 25-m long soft X-ray undulator and the monochromator is equipped with varied-line-spacing plain grating, which covers the photon energy range from 250 eV to 2 keV. At the end of the beamline, four experimental stations have been developed for frontier spectroscopy researches: the three-dimensional (3D) nano-ESCA station, the soft X-ray emission spectroscopy (XES) station, the time-resolved soft X-ray spectroscopy (TR-SX) station, and the free-port station for any experimental apparatus. The beamline construction was completed in 2009 and SRL established the Harima branch laboratory in SPring-8. The four end-stations have now been opened fully to outside users. In 2011, 110 researchers made their experiments during the SPring-8 operation time of 4000 hours.

Members of SRL have devoted themselves in serving users with technical supports and they have also carried out their own research works on advanced solid state spectroscopy. At SPring-8 BL07LSU, for example, the staffs have achieved the high performance at their stations: the 3D nano-ESCA reaches the spatial resolution of 70 nm, the XES station obtains spectra with energy resolving power $E/\Delta E$ larger than 10,000, and the TR-SX makes the laser-pump and SR-probe method with the time-resolution of 50 ps which corresponds to the SR pulse-width.

A few members of SRL have been dedicated to research works on the accelerator physics and developing various new accelerator related technology in collaboration with other SR facilities. They study future ERL (energy recovery linac) light source and developed ERL components in collaboration with KEK, the National Institute of Advanced Industrial Science and Technology (AIST) and Japan Atomic Energy Agency (JAEA), main works of which are carried out both in Kashiwa campus and at KEK in Tsukuba.



Fig. 5. TR-SX station at SPring-8 BL07LSU

Supercomputer Center

The Supercomputer Center (SCC) is a part of the Materials Design and Characterization Laboratory (MDCL) of ISSP. Its mission is to serve the whole community of computational condensed-matter physics of Japan providing it with high performance computing environment. In particular, the SCC selectively promotes and supports large-scale computations. For this purpose, the SCC invites proposals for supercomputer-aided research projects and hosts the Steering Committee, as mentioned below, that evaluates the proposals.

The ISSP supercomputer system consists of two subsystems: System A, which is intended for a parallel computation with relatively smaller number of nodes connected tightly, and System B, which is intended for more nodes with relatively loose connections. In July, 2010, the SCC replaced the two supercomputer subsystems. The new system B is SGI Altix ICE 8400EX, which consists of 30 racks or 15360 cores whereas the new system A is NEC SX-9, which consists of 4 nodes or 64 cpus. They have 200 TFlops in total.

On 11th Mar. 2011, the both systems were shut down owing to the Great East Japan Earthquake. Although they had no direct damage due to the earthquake, the systems had been suspended totally for one month and partially for five months because of power shortage. Normal full operation restarted in September 2011.

The hardware administration is not the only function of the SCC. The ISSP started hosting Computational Materials Science Initiative (CMSI), a new activity of promoting materials science study with next-generation parallel supercomputing. This activity is financially supported by the MEXT HPCI strategic program, and in CMSI, a number of major Japanese research institutes in various branches of materials science are involved. The SCC supports the activities of CMSI as its major mission.

All staff members of university faculties or public research institutes in Japan are invited to propose research projects (called User Program). The proposals are evaluated by the Steering Committee of SCC. Pre-reviewing is done by the Supercomputer Project Advisory Committee. In school year 2011, 200 projects in total were approved. The total points applied and approved are listed on Table 1 below.

Class	Max/Min Points	Application	Number of Projects	Total Points			
				Applied		Approved	
				System A	System B	System A	System B
A	<100	any time	4	0K	0.4K	0K	0.4K
B	<2K	twice a year	43	22.2K	58.0K	19.3K	27.6K
C	<20K	twice a year	146	619.3K	1878.5K	580.7K	509.0K
D		any time	6	4.0K	94.5K	2.5K	60.8K
S	>20K	twice a year	1	0K	40.0K	0K	10.5K
CMSI				-	-	-	114.5K
Total			200	645.5K	2071.4K	602.5K	722.8K

Table 1. Research projects approved in 2011

The maximum points allotted to the project of each class are the sum of the points for the two systems; Computation for 1 CPU-hour corresponds to 0.6 and 0.02 points for System-A and System-B, respectively.

The research projects are roughly classified into the following three (the number of projects approved):

First-Principles Calculation of Materials Properties (84)
Strongly Correlated Quantum Systems (53)
Cooperative Phenomena in Complex, Macroscopic Systems (63)

All the three involve both methodology of computation and its applications. The results of the projects are reported in 'Activity Report 2011' of the SCC. Every year 3-4 projects are selected for "invited papers" and published at the beginning of the Activity Report. In the Activity Report 2011, the following three invited papers are included:

"DFT-MD approach to TiO_2 /liquid interface systems for photocatalysis and dye-sensitised solar cell",
Yoshitaka TATEYAMA, Masato SUMITA, and Keitaro SODEYAMA
"Numerical Simulations of Electron-phonon Coupled Impurity Problems",
Kazumasa HATTORI
"Multiple- q states and skyrmion lattice in frustrated triangular-lattice Heisenberg antiferromagnet",
Tsuyoshi OKUBO and Hikaru KAWAMURA

Neutron Science Laboratory

The Neutron Science Laboratory (NSL) has been playing a central role in neutron scattering activities in Japan since 1961 by performing its own research programs as well as providing a strong General User Program for the university-owned various neutron scattering spectrometers installed at the Japan Research Reactor (JRR) -3 (20MW) operated by Japan Atomic Energy Agency (JAEA) in Tokai (Fig. 1). In 2003, the Neutron Scattering Laboratory was reorganized as the Neutron Science Laboratory to further promote the neutron science with use of the instruments in JRR-3. Under the General User Program supported by NSL, 14 university-group-owned spectrometers in the JRR-3 reactor are available for a wide scope of researches on material science, and proposals close to 300 are submitted each year, and the



Fig. 1. The reactor of JRR-3. The eight neutron scattering instruments are attached to the horizontal beam tubes in the reactor experimental hall. Two thermal and three cold guides are extracted from the reactor core towards the guide hall located to the left.



Fig. 2. The U.S.-Japan spectrometer, CTAX, installed at the cold guide line CG4, High Flux Isotope Reactor (HFIR), in Oak Ridge National Laboratory. Members who contributed the relocation project of the U.S.-Japan spectrometer celebrates the completion of the project in October 2010.)

number of visiting users under this program reaches over 6000 person-day/year. In 2009, NSL and Neutron Science Laboratory (KENS), High Energy Accelerator Research Organization (KEK) built a chopper spectrometer, High Resolution Chopper Spectrometer, HRC, at the beam line BL12 of MLF/J-PARC (Materials and Life Science Experimental Facility, J-PARC). HRC covers a wide energy and Q -range ($10\mu\text{eV} < \hbar\omega < 2\text{eV}$ and $0.02\text{\AA}^{-1} < Q < 50\text{\AA}^{-1}$), and therefore becomes complementary to the existing inelastic spectrometers at JRR-3. HRC started to accept general users through the J-PARC proposal system in FY2011.

Triple axis spectrometers, HRC, and a high resolution powder diffractometer are utilized for a conventional solid state physics and a variety of research fields on hard-condensed matter, while in the field of soft-condensed matter science, researches are mostly carried out by using the small angle neutron scattering (SANS-U) and/or neutron spin echo (iNSE) instruments. The upgraded time-of-flight (TOF) inelastic scattering spectrometer, AGNES, is also available through the ISSP-NSL user program.

On March 11, 2011, a great earthquake with Magnitude 9.0 hit North East Coast of Japan. Fortunately, JRR-3 was under regular inspection and no serious accidents or damages were reported. However, the lifeline of Tokai Village area was lost for more than two weeks, and it took more than two months before damage inspection of JRR-3 could be started. As of April of 2012, JRR-3 has not restarted yet. General User Program of 2011 was cancelled and that of 2012 has been suspended so far. In order to compensate the loss of the activity of NSL, a number of proposals accepted in 2011 were transferred to overseas owing to kind offer from the major facilities, namely, ORNL, ILL, ANSTO, and HANARO.

Research topics on the hard-condensed matter science cover stripe order in high- T_c superconductors, and closely related 2 dimensional systems, charge and orbital ordering in CMR manganites, quadrupolar ordering in rare-earth based intermetallic compounds, spin dynamics of low dimensional dimer systems, etc. On the other hand, the research topics on the soft-condensed matter science cover structural characterization of polymer gels, polymer blends, micelles, amphiphilic polymers, block copolymers, proteins, dynamics of brush-polymers on surface, slow dynamics of surfactants, pressure dependence of dynamics of amphiphilic membranes, and so on. Structural determination of high-strength polymer gels and studies on their deformation

mechanisms were carried out by SANS-U. In addition, there are a variety of activities on fundamental physics, neutron beam optics, developments of neutron scattering techniques.

The NSL also operates the U.S.-Japan Cooperative Program on neutron scattering, providing further research opportunities to material scientists who utilize the neutron scattering technique for their research interests. In 2010, relocation of the U.S.-Japan triple-axis spectrometer, CTAX, was completed, and it is now open to users (Fig. 2).

<http://neutrons.ornl.gov/instruments/HFIR/CG4C/>

The activity report on Neutron Scattering Research in JFY2011 is given in NSL-ISSP Activity Report vol. 18 (2011), which can be downloaded from the following URL, http://quasi.issp.u-tokyo.ac.jp/actrep/actrep-18-2011/index-rep_vol18.html

The list of publication is also given at, http://quasi.issp.u-tokyo.ac.jp/actrep/actrep-18-2011/index-pub_vol18.html.

International MegaGauss Science Laboratory

The objective of this laboratory (Fig. 1) is to study the physical properties of solid-state materials (such as semiconductors, magnetic materials, metals, insulators, superconducting materials) under ultra-high magnetic field conditions. Such a high magnetic field is also used for controlling the new material phase and functions. Our pulse magnets, at moment, can generate up to 87 Tesla (T) by non-destructive manner, and from 100 up to 730 T (the world strongest as an in-door experiment) by destructive methods.

They are opened for scientists both from Japan and from overseas, especially from Asian countries, and many fruitful results are expected to come out not only from collaborative research but also from our in-house activities. One of our ultimate goals is to provide the scientific users as our joint research with magnets capable of a 100 T, milli-second pulses in a non-destructive mode, and to offer versatile physical precision measurements. The available measuring techniques now involve magneto-optical measurements, cyclotron resonance, spin resonance, magnetization and transport measurements.

Our interests cover the study on quantum phase transitions (QPT) induced by high magnetic fields. Field-induced QPT has been explored in various materials such as quantum spin systems, strongly correlated electron systems and other



Fig. 1. Signboard at the entrance of the IMGSL.



Fig. 2. The building for the flywheel generator (left hand side) and a long-pulse magnet station (right hand side). The flywheel giant DC generator is 350 ton in weight and 5 m high (bottom). The generator, capable of a 51 MW output power with the 210 MJ energy storage, is planned to energize the long-pulse magnet generating 100 T without destruction.

magnetic materials. Non-destructive strong pulse magnets are expected to provide us with reliable and precise solid state physics measurements. The number of collaborative groups for the research is over 50 in the year of 2011.

A 210 MJ flywheel generator (Fig. 2) which is the world's largest DC power supply has been installed in the newly built DC flywheel generator station at our institute. The generator, once disassembled from the one used for Toroidal magnet coil in JFT-2M (JAERI Fusion Torus-2M) Tokamak nuclear fusion testing device, is now renewed as a power supply for the pulse magnets. The construction of the magnet service station has also been accomplished. The magnet technologies are intensively devoted to the quasi-steady long pulse magnet (an order of 1-10 sec) energized by the giant DC power supply. This DC generator is also used for supplying a current to a large-size outer-magnet coil of a dual coil to realize a 100 T nondestructive magnet.

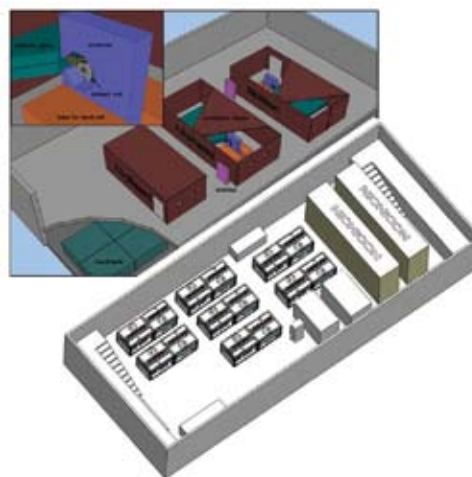


Fig. 3. (Build. C) The building for the electro-magnetic flux compression, generating over 700 T. 1000 T project started since 2010, and finally condenser banks of 9 MJ (5 MJ + 2 MJ + 2 MJ) as a main system with the 2 MJ sub bank system for the seed field will be installed, and will be completed in the year of 2013.

Developments of our destructive magnets are currently in progress. The ultra-high magnetic fields are obtained in a microsecond time scale. The electromagnetic flux compression (EMFC) system is equipped with a 5 MJ condenser bank and its seed coils with a 1.5 MJ condenser bank. The protector chamber and iron block protectors were refined against stronger explosion than before to be resistant against explosion by a full injection of 5 MJ. By devising copper lined primary coil, we could improve energy transfer efficiency from the primary coil to the liner kinetic energy compressing the magnetic flux. The seed field coils providing the initial magnetic flux are also newly designed and the maximum magnetic field was increased from 3.2 T to over 4.4 T at the position of the primary coil. These efforts led us to obtain the maximum magnetic field of 730 T by a 4 MJ injection of the EMFC recognized as a renewal of the world record as an indoor experiment. We have started a new project of the EMFC aiming at achieving 1000 T and its application to the materials science, financed by the ministry of education, culture, sports, science and technology in the 2010 and 2011 fiscal year (Fig. 3).

As an easy access to the megagauss science and technology, we have the single-turn coil (STC) system capable of generating the fields of up to 300 T by a fast-capacitor of 200 kJ. We have two STC systems, one is a horizontal type (H-type, Fig. 4) and the other is a vertical type (V-type). Various kinds of laser spectroscopy experiments such as the cyclotron resonance and the Faraday rotation using the H-type STC are available. On the other

hand, for a very-low temperature experiment, a combination of the V-type STC and a liquid helium bath cryostat is very useful; the precise magnetization measurements at 2.5 K can be performed up to 120 T.

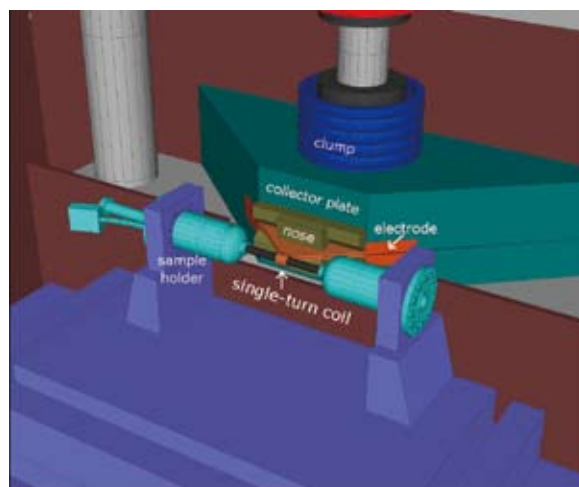


Fig. 4. Schematic picture of the H-type single-turn coil equipped with a 50 kV, 200 kJ fast operating pulse-power system, capable of generating 300 T within 3 mm bore coil.

	Alias	Type	B _{max}	Pulse width Bore	Power source	Applications	Others
Building C Room 101-113	Electro- Magnetic Flux Compression	destructive	730 T	μ s 10 mm	5 MJ, 40kV	Magneto-Optical Magnetization	5 K – Room temperature
	Horizontal Single-Turn Coil	destructive	300 T 200 T	μ s 5 mm 10 mm	0.2 MJ, 50 kV	Magneto-Optical measurements Magnetization	5 K – 400 K
	Vertical Single-Turn Coil	destructive	300 T 200 T	μ s 5 mm 10 mm	0.2 MJ, 40 kV	Magneto-Optical Magnetization	2 K – Room temperature
Building C Room 114-120	Mid-Pulse Magnet	Non-destructive	60 T	40 ms 18 mm	0.9 MJ, 10 kV	Magneto-Optical measurements Magnetization Magneto-Transport Hall resistance Polarization Magneto-Striction Magneto-Imaging Torque Magneto- Calorimetry Heat Capacity	Independent Experiment in 5 site Lowest temperature 0.1 K
			70 T	40 ms 10 mm			
Building C Room 121	PPMS	Steady State	14 T			Resistance Heat Capacity	Down to 0.3 K
	MPMS	Steady State	7 T			Magnetization	
Building K	Short-Pulse magnet	Non-destructive	87 T (2-stage pulse)	5 ms 10 mm 5 ms 18 mm	0.5 MJ, 20 kV	Magnetization Magneto-Transport	2K – Room temperature
	Long-Pulse magnet	Non-destructive	30 T	0.5 s 30 mm	210 MJ, 2.7 kV	Resistance Magneto-Calorimetry	2K – Room temperature

Table 1. Available Pulse Magnets, Specifications

Center of Computational Materials Science

K-computer at Kobe won the title of the world's fastest computer at TOP500 ranking announced at International Supercomputing Conference (ISC) 11. With the advancement of hardware and software technologies, large-scale numerical calculations have been making important contributions to materials science and will have even greater impact on the field in the near future. Center of Computational Materials Science (CCMS) was founded in April 2011 as a specialized research center for promoting computer-aided materials science with massively parallel computation using K-computer. This center is also the headquarters of Computational Materials Science Initiative (CMSI), which is an inter-institutional organization for computational science of a broad range of disciplines, including molecular science, quantum chemistry, biological materials, and solid state physics. ISSP made contracts with 9 universities and 2 national institutes for supporting the activities of CMSI in which nearly 100 research groups are involved. The main purpose of CMSI is to establish a new community of computational science in which researchers from different backgrounds work together on grand challenge problems, thereby developing computational infrastructures (new algorithms, coding styles, standard software packages, etc) and inspire young scientists.

A branch office of CCMS was also established in the RIKEN AICS building on Port Island (Kobe), where K-computer is located, for supporting CMSI researchers getting together at Kobe to fine-tune various applications software for K-computer, and developing collaborations with staff members of RIKEN, the operating institute of K-computer. Another mission of the Kobe branch of CCMS is exchanging ideas and techniques with researchers from other fields of computer science. (There are 5 major fields in the HPCI strategic program of MEXT, "biology", "materials and energy" (our field), "seismology, oceanography and meteorology", "industrial applications", and "high-energy physics and cosmology".) In October 2011, Professor Todo was appointed to direct the Kobe branch, for coordinating activities of researchers from all over the country.



Fig. 1. K-Computer



Fig. 2. CMSI researchers at AICS, Kobe.

The following is a selected list of meetings organized by CMSI and CCMS in SY2011:

- "Programming Techniques for K-Computer"
(July 7-8, 2011, AICS)
- "Joint-Meeting between Field 2 and 5"
(July 26, Tsukuba)
- "Rare-Elements Related Science --- Magets"
(July 29, Hongo)
- "CCMS Symposium --- Collaborations Among National Facilities"
(September 12-13, ISSP)
- "Programming Techniques for K-Computer"
(September 14, ISSP)
- "Rare-Elements Related Science --- Batteries"
(November 9, Hongo)
- "Rare-Elements Related Science --- Catalyst"
(November 12, Kyoto)
- "Programming Techniques for K-Computer"
(November 25, Komaba)
- "Rare-Elements Related Science --- Electronic Devices"
(December 5, Hongo)
- "CMSI Symposium"
(January 30-31, Sendai)
- "Programming Techniques for K-Computer"
(February 1, Sendai)
- "Programming Techniques for K-Computer"
(March 12-14, Atami)
- "How to use K"
(May 10, 2012, AICS)

Giant Negative Thermal Expansion in SrCu₃Fe₄O₁₂

I. Yamada and K. Ohgushi

We have synthesized a novel Fe⁴⁺-perovskite SrCu₃Fe₄O₁₂ (SCFO) using high pressure synthesis method (15GPa, 1000 °C) [1]. This compound consists of pseudo-square-coordinated Cu²⁺ ions and unusual high valence Fe⁴⁺ ions with octahedral coordination. Synchrotron powder X-ray diffraction (SXRD) data demonstrated a negative thermal expansion (NTE) in temperature range of 170–270 K (Fig. 1). The maximum value of the linear expansion coefficient (α) is $\alpha = -2.26 \times 10^{-5} \text{ K}^{-1}$ (Fig. 2(a)), which is comparable with the highest value ($\alpha = -2.5 \times 10^{-5} \text{ K}^{-1}$) for an antiperovskite nitride [2]. To our knowledge, this is the first observation of giant NTE in iron-based compounds.

Rietveld refinement based on the SXRD data indicates that the origin of the giant NTE in SCFO is a crossover-like intersite charge transfer between Cu and Fe. The bond valence sums (BVS) for Cu and Fe calculated from the metal–oxygen bond lengths (Fig. 2(b)) gradually change from +2.21 (Cu) and +3.54 (Fe) at 300 K to +2.99 (Cu) and +3.24 (Fe) at 80 K. The decreased nominal valence of Fe ion was confirmed by Mössbauer spectroscopy. The charge-disproportionated transition was observed below ~200 K with an abundance ratio of Fe³⁺:Fe⁵⁺ \doteq 4 : 1 at 4 K. This indicates that the nominal valence of Fe is \sim +3.4 at ~200 K, as expected from the charge disproportionation transition of 5Fe^{3.4+} \rightarrow Fe⁵⁺ + 4Fe³⁺.

The expansion of the lattice constant a on cooling in NTE temperature range is attributed to the elongation of Fe–O bond length ($d_{\text{Fe-O}}$) based on the crystallographic relation of $a = 4d_{\text{Fe-O}} \times \sin(\psi/2)$, where $\psi/2$ is a Fe–O–Fe bond angle. The NTE behavior of SCFO is clearly distinguished from an abrupt volume expansion in LaCu₃Fe₄O₁₂ (LCFO) [3] (Fig. 2(a)). This demonstrates the versatility of structural and electronic properties in the Fe⁴⁺-perovskite oxides. We are now studying A-site cation substitution effect of ACu₃Fe₄O₁₂ perovskite further in order to clarify the relationship between crystal structure and electronic property.

References

[1] I. Yamada, K. Tsuchida, K. Ohgushi, N. Hayashi, J. Kim, N. Tsuji, R. Takahashi, M. Matsushita, N. Nishiyama, T. Inoue, T. Irifune, K. Kato, M. Takata, and M. Takano, *Angew. Chem., Int. Ed.* **50**, 6579 (2011).

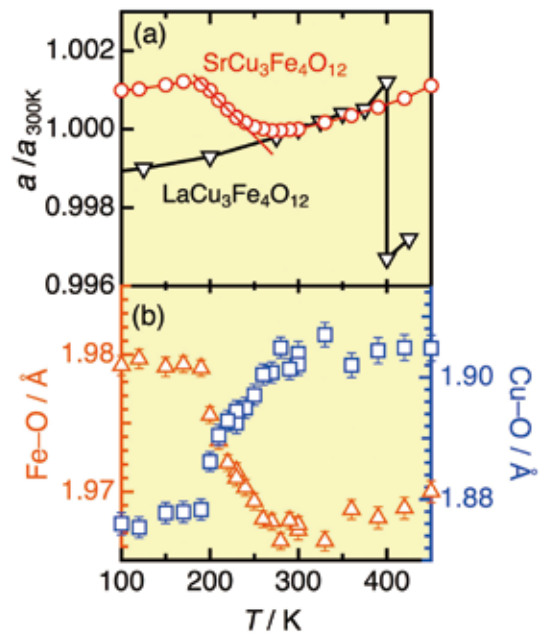


Fig. 2. (a) Temperature dependence of (a) the lattice constant normalized at 300 K ($a/a_{300\text{K}}$) compared with that of LaCu₃Fe₄O₁₂ [3] and (b) the metal–oxygen bond length.

[2] K. Takenaka and H. Takagi, *Appl. Phys. Lett.* **87**, 261902 (2005).

[3] Y. W. Long, N. Hayashi, T. Saito, M. Azuma, S. Muranaka, and Y. Shimakawa, *Nature* **458**, 60 (2009); W. Chen, Y. Long, T. Saito, J. P. Attfield, and Y. Shimakawa, *J. Mater. Chem.* **20**, 7282 (2010).

Authors

I. Yamada^{a,b}, K. Tsuchida^b, K. Ohgushi, N. Hayashi^c, J. Kim^d, N. Tsuji^d, R. Takahashi^b, M. Matsushita^b, N. Nishiyama^b, T. Inoue^b, T. Irifune^b, K. Kato^e, M. Takata^e, and M. Takano^c

^aOsaka Prefecture University

^bEhime University

^cKyoto University

^dJASRI

^eRIKEN

Superfluid-Mott-Insulator Quantum Phase Transition of Light in the Jaynes-Cummings Lattice

H. Zheng and Y. Takada

Quantum phase transitions and related phenomena constitute a field of great interest in the physics of strong correlation. Recently, the Jaynes-Cummings lattice (JCL) attracts much attention in this field, partly because it is a good model system for studying strongly correlated polariton physics and partly because it offers potential use of a quantum simulator for solid-state Hamiltonians, just like the cold-atom systems.

The JCL model is composed of a lattice of electromagnetic micro-cavities with frequency ω , each coupled to a two-level atom with level spacing ϵ , and the intrasite atom-photon coupling g is competed with the intersite photon hopping J . A mean-field treatment of the model reveals a phase transition from Mott insulator (MI) to superfluid phase, resembling in large parts the phase diagram of the Bose-Hubbard model with an eminent feature of the Mott lobes at the boundary between the insulating phase and the superfluid one (See Fig. 1). Both numerical and analytical methods have been employed to study the phase diagram as well as the spectra of low-lying excitations beyond the mean-field approximation and confirmed the existence of the

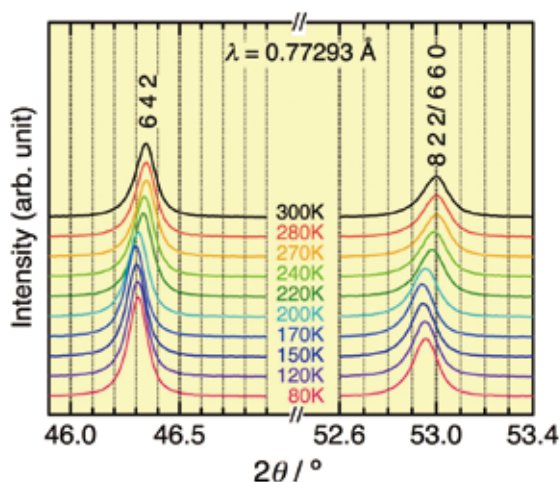


Fig. 1. SXRD patterns of SrCu₃Fe₄O₁₂ in the vicinity of 6 4 2 and 8 2 2 / 6 6 0 Bragg reflections between 80 and 300 K.

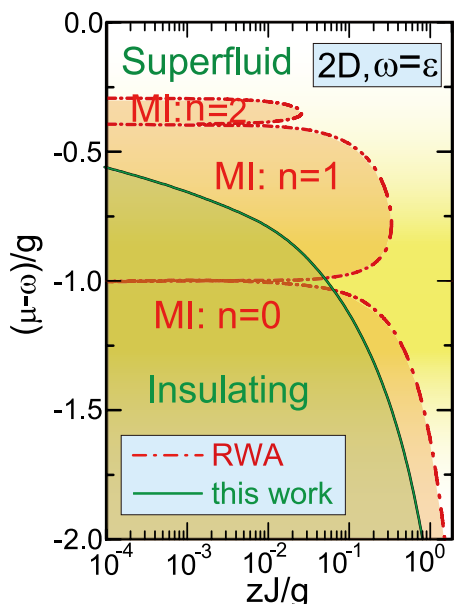


Fig. 1. Phase diagram in the $[(\mu-\omega)/g, zJ/g]$ space, or the particle average number vs intersite coupling strength J in units of the atom-photon coupling g , for the two-dimensional square JCL at the resonant condition of $\omega = \epsilon$, where z is the coordination number. The inclusion of the usually neglected counter-rotating term makes such a radical change in the phase diagram; in particular, the eminent Mott lobes are eliminated.

Mott lobes.

All those theoretical studies, however, have not been done on the physically correct original JC model but under the rotating-wave approximation (RWA), in which the Hamiltonian H_{RWA} commutes with the polariton number operator N_p at each lattice site, leading to the conservation of the local polariton number as specified by the chemical potential μ . This conservation law is, in fact, a key feature to provide the Mott lobes in the phase diagram.

The counter-rotating (CR) term H_{CR} , included in the original JCL model but neglected so far, will be irrelevant in resonance experiments to detect real transitions, but this will be physically relevant in virtual transitions in the formation of the ground state, making the RWA for the JCL model less reliable in describing the ground-state properties, especially for g of the order of ω and/or ϵ . Besides, H_{CR} breaks the conservation of the local polariton number, i.e., $[H_{CR}, N_p] \neq 0$, implying a radical change of the phase diagram, once the CR is included. Moreover, H_{CR} induces an additional long-range interaction between cavities, enhancing a long-range ordering in the JCL model.

Here we have studied the effects of H_{CR} on the quantum phase transition of light in the two-dimensional (2D) square JCL with H_{CR} faithfully included. The ground state as well as spectra of low-lying excitations in both the insulating and the superfluid phases is investigated with use of a sophisticated unitary transformation, which has been developed in the polaron physics. The obtained phase diagram is shown in Fig. 1, indicating that the Mott lobes are absent in sharp contrast with the case of RWA. Thus we may conclude that the physics of the JCL is basically different from that of the Bose-Hubbard model as opposed to the conclusion drawn in the preceding works.

Finally we find that gapped excitations appear even in the superfluid phase in our calculation. Note that for the JCL in the RWA as well as the Bose-Hubbard model, the particle number conservation is broken by the superfluid transition, leading to the gapless bosons according to the Goldstone theorem, but if H_{CR} is included, the number conservation

is broken from the outset, making our system stay outside of the Goldstone theorem. In our superfluid transition, the discrete parity conservation law is broken spontaneously, instead.

Reference

[1] H. Zheng and Y. Takada, Phys. Rev. A 84, 043819 (2011).

Authors

H. Zheng^a and Y. Takada
^aShanghai Jiao Tong University

Refined First-Principles Computational Scheme for the Electrode Dynamics

M. Otani, N. Bonnet, and O. Sugino

The problem of the bias-potential induced charge-transfer dynamics and associated structural change at the solid-liquid interface has attracted renewed attention. This problem, known as the *electrode problem*, has been recognized since the invention of the fuel-cell in 19th century and is focused today as a key issue in the development of clean energy-conversion devices. Atomic scale details, however, have remained only imperfectly elucidated. The authors worked together until several years ago as a member of this institute and developed a method to apply the bias-potential to the interface. The method, which is called the Effective Screening Medium (ESM) [1], was implemented to a first-principles molecular dynamics (FPMD) simulation code and was used to successfully detail the atomistic processes on the platinum electrode, where the hydrogen-evolution is initiated by an exchange of the electron and the hydrated proton (or the hydronium ion: H_3O^+) [2]. Because of the generation change of the supercomputer, the computational speed has been increased by two orders of magnitude since that time, and it has now become possible to dramatically enhance the accuracy of the simulation. In this context, the authors developed schemes to sophisticate the ESM simulation.

There are two major improvements. One is related to the ESM modeling of bulk water. In the original ESM, the water molecules beyond those explicitly treated were modeled by

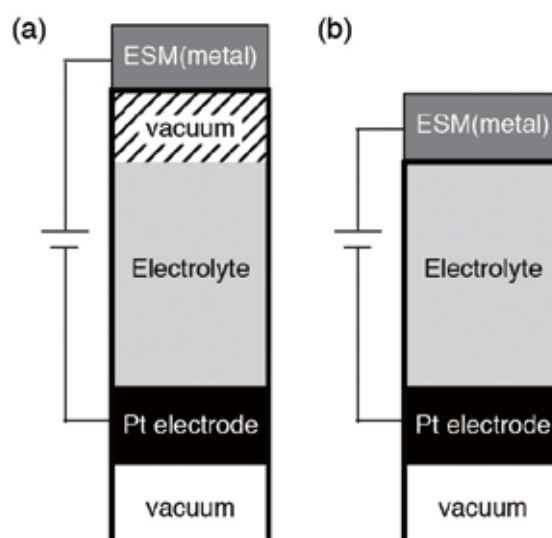


Fig. 1. Schematic configurations of (a) original and (b) smooth ESM. By introducing the improved algorithm, we can remove undesirable vacuum region (hatched region in (a)).

the dielectric continuum, but a thin vacuum region (hatched area in fig. 1(a)) had to be inserted in between because of an algorithmic reason. The existence of vacuum region degraded the simulation hindering the interpretation of the calculated results. The vacuum region is found dispensable when the border is smoothed by introducing an improved algorithm. The refined ESM, called smooth ESM, allows us to construct more realistic modeling of the electrode/electrolyte interface (see fig1.(b)). It is coded and tested to show that the description of the border greatly improved.

The other improvement is on the FPMD simulation. It is desirable to conduct the simulation keeping the bias-potential constant as does a real electrode, but our former simulation was done under the constant charge condition. To switch the scheme from the constant charge to the constant bias-potential, we introduce a double thermostat to keep both bias-potential and temperature constant. When implemented in our code to test an interface, the scheme is found to work indeed without making the simulation unstable.

Our joint group is selected as a priority subject in the “K-computer” project. With the refined simulation scheme, we will soon start using the extraordinary computational facility to attack the electrode problem.

References

- [1] M. Otani and O. Sugino, Phys. Rev. B **73**, 115407 (2006).
 [2] M. Otani, I. Hamada, O. Sugino, Y. Morikawa, T. Ikeshoji, and Y. Okamoto, J. Phys. Soc. Jpn. **77**, 024802 (2008).

Authors

M. Otani^a, N. Bonnet, and O. Sugino

^aNational Institute of Advanced Industrial Science and Technology

Spontaneous Spin Polarization on Pore Edges of Graphene Nanomesh

K. Tada, J. Haruyama, and Y. Iye

Graphene, an ultimate two-dimensional molecule sheet with thickness as thin as one carbon atom size, is attracting significant attention. Although a variety of attractive phenomena has been experimentally reported in graphenes, none has experimentally reported on edge-related phenomena. Basically, there are two kinds of atomic structures of graphene edges; i.e., arm chair and zigzag edges. Theoretically, arm chair edge introduces energy band gap to graphenes, while zigzag edge yields a flat energy band, which makes electrons localize around the edge. The localized electrons are spontaneously spin-polarized due to strong electron interaction arising from extremely high electron density of states (i.e., edge states). It allows research of spin-based phenomena and those applications to novel spintronic devices in spite of a material consisting of only carbon atoms with sp^2 orbitals. None has, however, reported on experimental observation of edge-related phenomena, because lithographic fabrication of graphene edges easily introduces defects. Only our group reported on finding of large energy band gaps in low-defect graphene nanoribbons (one-dimensional strip lines of graphenes with two edges along the longitudinal direction), which were fabricated by a non-lithographic method (i.e., derived from unzipping of carbon nanotubes) [1].

Here, we report on the other non-lithographic fabrication of graphene edges (Figure 1(a); graphene nanomesh with a honeycomb like array of hexagonal nanopores, which

was fabricated using nano-porous alumina template as an etching mask). The method and system allow formation of a large ensemble of low-disorder nanopore edges and nanoribbons (i.e., inter-pore regions). Figure 1(b) shows a result of magnetization measurement of the nanomeshes with hydrogen (H)-terminated zigzag pore edges at room temperature. A ferromagnetic hysteresis loop with large amplitude is clearly observed. In contrast, this feature becomes a diamagnetism like weak hysteresis loop for oxygen-terminated nanomeshes. Bulk graphenes without nanopores show mostly no such features. Observation by magnetic force microscope for the Fig.1(b)-sample is shown in Fig.1(c). Higher densities of spins are evidently confirmed at the inter-pore regions (nanoribbon regions) and also some parts of pore edges (shown by arrows). These results imply that the observed ferromagnetism originates from the H-terminated nanopore edges and also the nanoribbons sandwiched by the pore edges. The observed magnetization value of $\sim 0.3\mu_B$ per one edge dangling bond is also in quantitatively good agreement with predictions of two theories (i.e., nanoribbon model and Lieb’s theorem).

We cannot yet control fabrication of the zigzag atomic

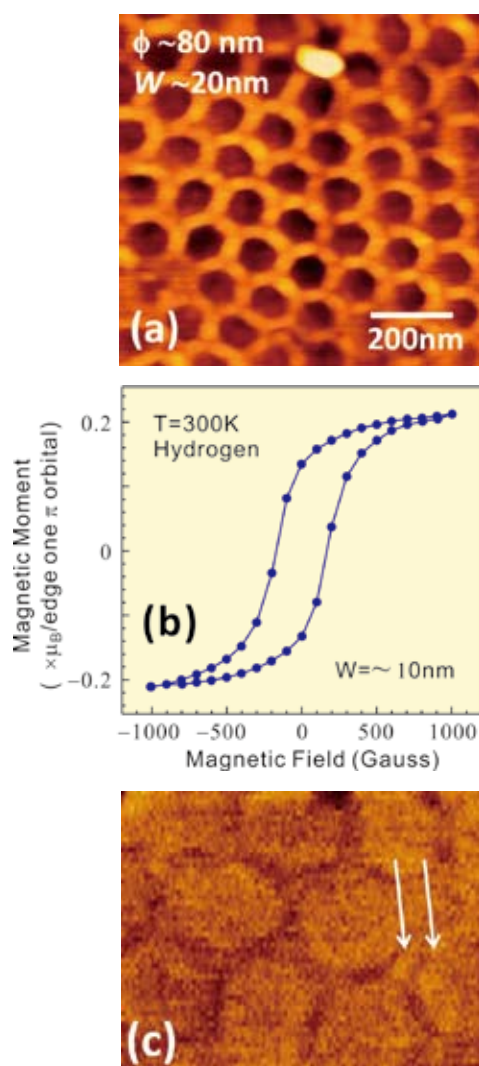


Fig. 1. (a) AFM image of a graphene nanomesh with a honeycomb like array of hexagonal nanopores. It was formed by optimized low-power Ar-gas etching using a nano-porous alumina template as a mask. Mean pore diameter ϕ and inter-pore distance W are ~ 80 nm and ~ 20 nm, respectively. (b) Room-temperature magnetization of hydrogen-terminated nanomesh measured by a superconducting quantum interference device (Quantum Design). (c) Magnetic force microscope image of (b)-sample. Darker parts mean presence of polarized electron spins. Arrows indicate polarized spins existing at pore edges.

structure of the pore edges. We are just selecting the nanomeshes, which exhibited low D peaks in Raman spectrum after annealing, for the measurement, because it indirectly proves presence of zigzag pore edges. Exact observation of atomic structure of pore edges and its control are indispensable in near future. It is highly expected that the present graphene nanomesh can realize a high-efficiency graphene magnet, which is ultra-light (wearable), flexible, invisible, and rare-element free. Modulating a flat band and introducing polarized spins from pore edges to bulk graphene regions will also open a door to novel all-carbon spintronic devices with strong spin coherence.

Reference

[1] T.Shimizu, J.Haruyama *et al.*, Nature Nanotech. 6, 45 (2011) (Selected for Latest highlights, News & Views, and Cover index).

Authors

K. Tada^a, J.Haruyama^a, and Y. Iye^a
^aAoyama Gakuin University

Uniaxial Deformation of Graphene Dirac Cone on a Vicinal SiC Substrate

S. Tanaka and F. Komori

Modification of gapless graphene Dirac band has been widely investigated for understanding electronic properties characteristic to their chiral nature and for their useful applications. In the case of graphene on substrates, its electronic states can be changed by controlling the substrate nanostructure. We have studied the electronic states of graphene grown on the SiC(0001) substrates with step-and-terrace structures using angle-resolved photoemission spectroscopy (ARPES). On this substrate, high-quality graphene is prepared by thermal decomposition, and covers the whole surface continuously including the step edges. We found that the Dirac band is uniaxially deformed in the wave-number space for the substrate with narrow terraces. This is consistent with theoretical results that the group velocity of the Dirac electrons can be tuned anisotropically by external potentials in a nanometer scale [1,2].

Single-layer graphene was made by annealing Si-terminated surfaces of nitrogen-doped 6H- and 4H-SiC(0001) substrates vicinal to the $[1\bar{1}00]$ direction. The tilting angle was either 4 (6H) or 8 (4H) degree. The terraces are elongated in the direction perpendicular to $[1\bar{1}00]$ as confirmed by scanning probe microscopes. The terrace widths in the $[1\bar{1}00]$ direction were 21 and 9 nm on average for the 4°- and 8°-off substrates, respectively, while the width perpendicular to the $[1\bar{1}00]$ direction was commonly 100 nm. Figure 1 shows the results of the STM observation at 80 K for the graphene on the 8°-off substrate. The graphene at the substrate step edge is curved as observed by STM, and connects the flat graphene on the adjacent terraces. Namely, the present system consists of flat graphene on the terrace and curved one in the vicinity of the step edges. Electrons in the Dirac band on the terrace are scattered at the curved area of graphene as previously confirmed. [3]

The shapes of the graphene π and π^* bands were studied using ARPES. The Dirac point was 0.4 eV below Fermi energy E_F because of the doping from the substrate as in the case of the flat SiC substrate. For the graphene on the 4°-off substrate, the observed constant-energy ARPES intensity maps indicate trigonally-warped π and π^* bands, and agree

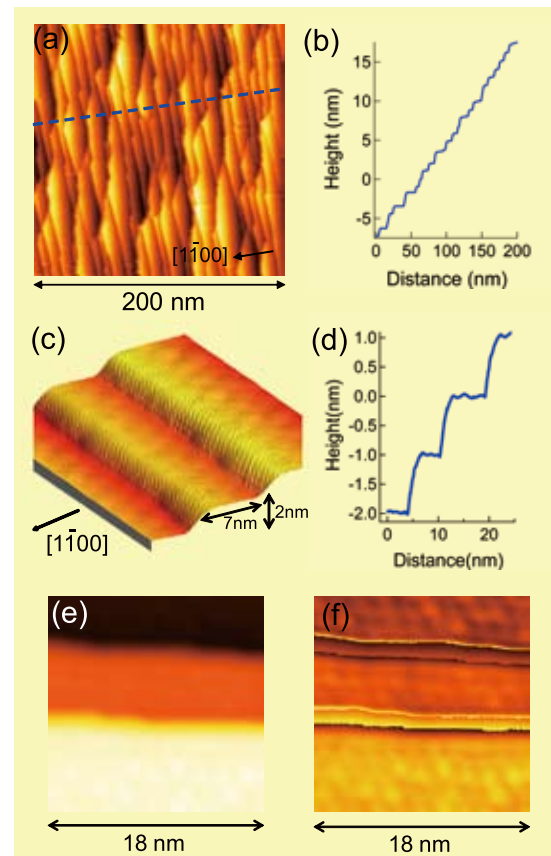


Fig. 1. Results of STM observations for the graphene grown on the 8°-off SiC(0001) substrate tiling toward $[1\bar{1}00]$ direction. Topographic STM images (a,e) show a step-and-terrace structure in wide (a) and narrow (e) areas. A three-dimensional illustration of the topographic STM image is shown in (c). In (f), atomic images of the substrate terraces are superimposed on (e). A honeycomb lattice with $6\sqrt{3} \times 6\sqrt{3}$ modulation can be seen on the terrace without point defects as in (c) and (f). This indicates the presence of well-ordered single-layer graphene, and the $6\sqrt{3} \times 6\sqrt{3}$ modulation is attributed to the interface reconstruction of the SiC(0001) substrate. Graphene continuously covers the step-edge area as in (c). Cross sections of the STM topographic image are shown in (b) and (d). The curve in (b) is along the dotted line in (a), and that in (d) includes three steps of 1 nm high. This step height corresponds to the unit length of the 4H-SiC crystal. The step-and-terrace structure is homogeneous in the area of $3 \text{ mm}\phi$ of the sample surface.

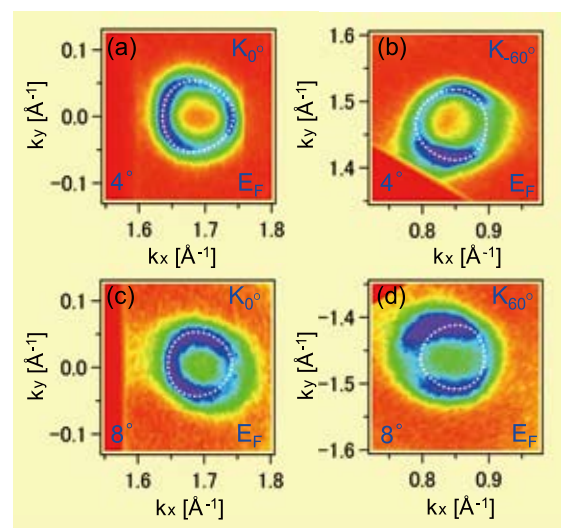


Fig. 2. Constant-energy ARPES intensity maps at E_F for the graphene samples formed on the 4°- (a,b) and 8°-off (c,d) substrates around K_0° (a,c), K_{60° (b), and K_{60° (d). Here 0 degree indicates the $[1\bar{1}00]$ direction. Dotted curves represent the constant-energy ideal band shape including the trigonal warping for flat graphene. The observed shape of the Dirac band for the 4°-off substrate is consistent with the ideal graphene while that for the 8°-off substrate is elongated in the $[1\bar{1}00]$ direction.

with the previous results. In contrast, the bands for the 8°-off substrate are significantly elongated in the [1100] direction. Figure 2 shows the comparison of the band shapes at E_F . The group velocity of the π^* band in the Γ -K direction parallel to [1100] for the 8°-off substrate is more than 15 % lower than the velocity in the other Γ -K directions. The velocity significantly reduces only in the direction parallel to the substrate slope consistently with the theoretical prediction due to deformation of graphene [2].

References

- [1] C.-H. Park *et al.*, Nat. Phys. **4**, 213 (2008).
- [2] S. Okada and T. Kawai, Jpn. J. Appl. Phys. **51**, 02BN05 (2012).
- [3] K. Nakatsuji *et al.*, Phys. Rev. B **82**, 045428 (2010).

Authors

K. Nakatsuji, T. Yoshimura, K. Morita^a, S. Tanaka^a, and F. Komori^a
^aKyushu University

Ferroelectric Double Perovskites

I. Ohkubo and R. Takahashi

Various double perovskites with ordered B-site lattices and a general formula of $A_2M'M''O_6$ have recently been synthesized and characterized. The magnetic behavior of these materials is particularly interesting, with half-metallic behavior in Sr_2FeMoO_6 , multiferroicity in Bi_2NiMnO_6 and Bi_2CoMnO_6 , and semiconducting ferromagnetism in La_2NiMnO_6 and La_2CoMnO_6 . The purpose of this joint-use project was to perform structural and dielectric characterization on La_2NiMnO_6 (LNMO) thin films that are semiconducting but become ferromagnetic at an exceptionally high temperature of 280 K. The material is thus a prime candidate for use in room-temperature spintronic device applications. Due to the ordered state of B-site cations with different valence states, such as Ni^{2+} and Mn^{4+} in La_2NiMnO_6 , double

perovskites are also prime candidates for strong magnetodielectric coupling, where the dielectric behavior can be controlled by applied magnetic fields. Due to the semiconducting behavior of La_2NiMnO_6 , however, accurate dielectric characterization close to the onset of magnetic order is hampered by the large conductivity. Our purpose, therefore, was to use zero-bias pyroelectric characterization to determine if a polar state exists in La_2NiMnO_6 , and to determine if this material might also show a switchable multiferroic response.

The ordering of the transition metal ions in double perovskites is often incomplete. It is therefore important to determine the structural quality of a crystal before dielectric measurements. The structural analysis was done by conventional x-ray diffraction and reciprocal space mapping analysis, as illustrated for a well-ordered sample in Fig. 1(a). It is clear that the La_2NiMnO_6 film is coherently grown on the $SrTiO_3$ substrate and the odd-index superlattice peaks characteristic of an ordered phase are clearly visible in an asymmetric diffraction pattern measured for a (001)-oriented thin film sample. The presence of the expected anisotropic polarization-dependent Raman scattering peaks was also verified for the same thin film samples.

The dielectric characterization was done in a planar capacitor geometry. The temperature dependence of the dielectric permittivity, measured at various frequencies, showed a clear relaxor-like behavior between 100 and 200 K. The pyroelectric measurements were done in the same capacitor geometry, using a chopped laser source for periodically heating and cooling the thin film capacitor. For polar materials, the small temperature modulation results in a change of the surface charge due to a temperature dependence of the spontaneous polarization. Since no bias is applied to a sample during the pyroelectric measurement, it is possible to determine the presence of a polar state even for a semiconducting material, where traditional ferroelectric testing would not be possible due to large leak currents. The measurements showed that a polar state does indeed appear in La_2NiMnO_6 at temperatures below 250 K. The pyroelectric coefficient can be determined from slow temperature sweeps, as illustrated in Fig. 1(b) and looking at the normalized slope of the thermally-induced current as a function of the sweep rate. Analysis of the data in Fig. 1(c) showed that the pyroelectric response in La_2NiMnO_6 is $34 \text{ nC/cm}^2\text{K}$, which is comparable to the well-known lead titanates. This study shows that ordered perovskites, like La_2NiMnO_6 , may be useful not only as spintronic materials, but may also be useful for developing lead-free pyroelectric sensors.

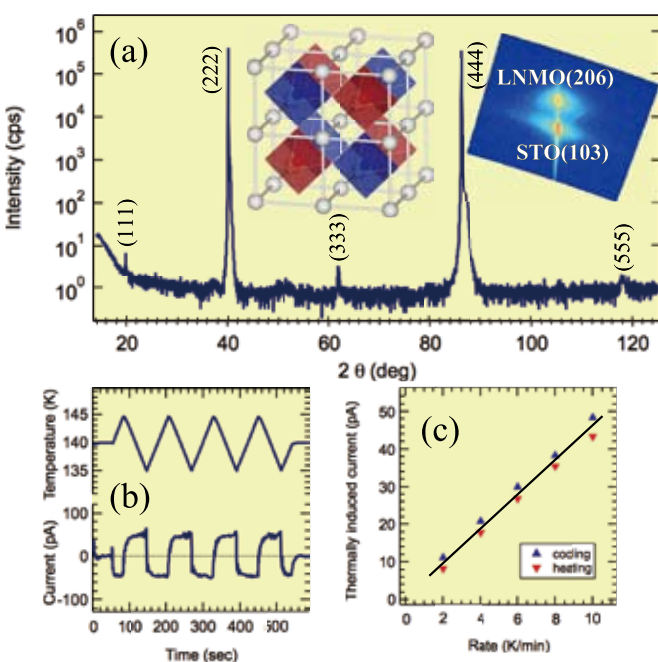


Fig. 1. X-ray diffraction analysis of an ordered perovskite La_2NiMnO_6 thin film sample. The reciprocal space mapping in the inset shows that the film is coherent on the $SrTiO_3$ substrate. Clear odd-index superlattice peaks due to B-site ordering are visible in the asymmetric diffraction pattern (a). The pyroelectric response of La_2NiMnO_6 is shown in (b), together with a rate-dependent thermally-induced current plot in (c).

Authors

I. Ohkubo^a, M. Oshima^a, R. Takahashi, and M. Lippmaa^a
^aDepartment of Applied Chemistry, University of Tokyo

Hall Coefficient of $CeRu_2Al_{10}$ under Pressure and of $Ce(Ru_{1-x}Fe_x)_2Al_{10}$ ($0 \leq x \leq 1$)

Y. Kawamura and Y. Uwatoko

The interaction between the local 4f electrons and the conduction electrons, namely c-f hybridization, brings about various physical properties such as Kondo semiconductor and long range order (LRO). Kondo semiconductor and LRO are incompatible with each other. The former happens in the 4f itinerant-electrons system and the latter happens in the 4f

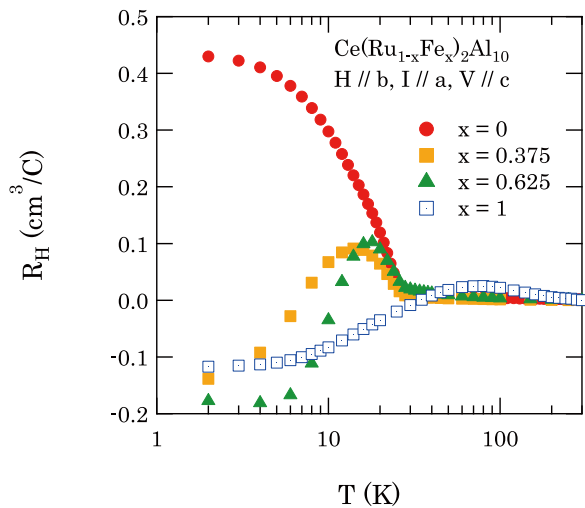


Fig. 1. Temperature dependence of Hall coefficient R_H on $\text{CeRu}_2\text{Al}_{10}$ under pressure.

localized-electrons system.

$\text{CeT}_2\text{Al}_{10}$ ($T=\text{Fe, Ru, Os}$) system is attracted much attention because of their unusual features such as unusual long range order (LRO) appeared in $\text{CeRu}_2\text{Al}_{10}$ at $T_0 \sim 27$ K [1] or in $\text{CeOs}_2\text{Al}_{10}$ [2] at $T_0 \sim 29$ K and Kondo semiconducting behavior appeared in $\text{CeFe}_2\text{Al}_{10}$ [3] or in $\text{CeOs}_2\text{Al}_{10}$. LRO and Kondo semiconductor may coexist in the same system. In addition, the temperature of LRO of $\text{CeRu}_2\text{Al}_{10}$ is extremely high in comparison with antiferromagnetic ordering temperature $T_N = 16.5$ K on $\text{GdRu}_2\text{Al}_{10}$ or $T_N = 2.4$ K on $\text{NdRu}_2\text{Al}_{10}$ which expected much higher than T_N of $\text{CeRu}_2\text{Al}_{10}$. In spite of high ordering temperature, magnetic moment in the ordered phase is reduced to $0.34\mu_B/\text{Ce}$ [4]. One of the key mechanisms behind this long range order is the gap open at T_0 . Hall coefficient R_H on $\text{CeRu}_2\text{Al}_{10}$ increases by nearly two orders of magnitude below T_0 before saturating towards low temperatures. In order to investigate the gap open at T_0 on $\text{CeRu}_2\text{Al}_{10}$ or Kondo semiconducting gap open on $\text{CeFe}_2\text{Al}_{10}$ from the viewpoint of physical pressure and chemical pressure, we measured Hall Resistivity on $\text{CeRu}_2\text{Al}_{10}$ under pressure and of $\text{Ce}(\text{Ru}_{1-x}\text{Fe}_x)_2\text{Al}_{10}$.

Figure 1 shows temperature dependence of Hall coefficient on R_H on $\text{CeRu}_2\text{Al}_{10}$ under pressure. The magnitude of R_H at lowest temperatures decreases with increasing pressure, which indicates that the gap open at T_0 shallows with pressure. Figure 2 the temperature dependence of

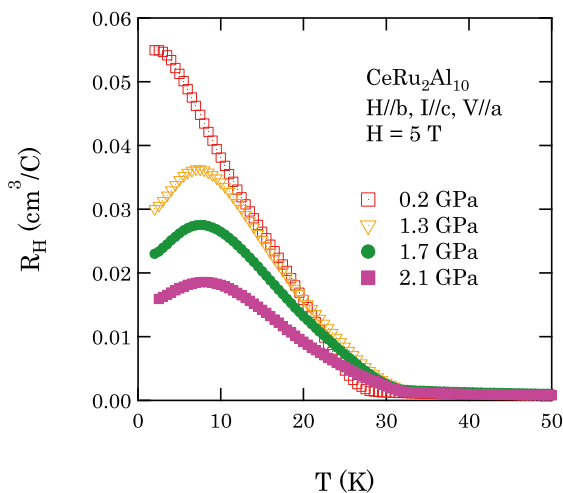


Fig. 2. Temperature dependence of Hall coefficient R_H on $\text{Ce}(\text{Ru}_{1-x}\text{Fe}_x)_2\text{Al}_{10}$.

Hall coefficient R_H on $\text{Ce}(\text{Ru}_{1-x}\text{Fe}_x)_2\text{Al}_{10}$. For $x=0.375$ and $x=0.625$, R_H increases abruptly below T_0 and become negative value at low temperatures, which indicates the gap open at T_0 in $\text{CeRu}_2\text{Al}_{10}$ exhibit as positive value of R_H and the c-f hybridization gap proposed in $\text{CeFe}_2\text{Al}_{10}$ exhibit as negative value. In addition, the reversal of the sign indicates that $\text{Ce}(\text{Ru}_{1-x}\text{Fe}_x)_2\text{Al}_{10}$ is in a multi-carrier system. The R_H of $\text{CeRu}_2\text{Al}_{10}$ are suppressed by pressure and the R_H of $\text{Ce}(\text{Ru}_{1-x}\text{Fe}_x)_2\text{Al}_{10}$ are suppressed by Fe substitution. The consistency of chemical pressure and physical pressure is observed in the Hall Effect measurement.

References

- [1] A. M. Strydom, *Physica B* **404**, 2981 (2009).
- [2] Y. Muro *et al.*, *J. Phys. Soc. Jpn.* **78**, 083707 (2009).
- [3] T. Nishioka *et al.*, *J. Phys. Soc. Jpn.* **78**, 123705 (2009).
- [4] D. D. Khalyavin *et al.*, *Phys. Rev. B* **82**, 100405 (2010).

Authors

Y. Kawamura^a, D. Hirai^b, T. Nishioka^b, D. Tanaka^c, H. Tanida^c, M. Sera^c, M. Matsubayashi, Y. Uwatoko
^aMuroran Institute of Technology
^bKochi University
^cHiroshima University

Two-Band Gap Superconductivity in LaRu_2P_2

T. Fujiwara and Y. Uwatoko

The recent discovery of superconductivity iron arsenide family has lead to wide research activities in advanced solid state physics. So far, lots of iron arsenide intermetallics family have been synthesized and investigated their physical properties, especially, characteristics of their superconductivity since the recent discovery of superconductivity in $\text{LaFeAs}(\text{O},\text{F})$ compound [1]. Both structure and symmetry of superconducting gap are often studied and argued to clarify the origin of their superconductivity with significantly high superconducting transition temperature in various kinds of Fe-As based compounds.

We paid our attention on ternary phosphide LaRu_2P_2 which is one of related material of iron arsenides superconductors crystallize in the ThCr_2Si_2 type structure. This compound shows a superconductivity below $T_c \sim 4.4$ K [2] and an upper critical fields H_{c2} vary isotropically with increasing or/and decreasing temperature. In addition, LaRu_2P_2 single crystal obtained in this work exhibits remarkably larger H_{c2} than that expected from GL theory at considerably low temperature, suggesting that this system is not conventional type II superconductor. So, we investigated a calorimetric characteristics in ternary phosphide LaRu_2P_2 in this work.

Temperature dependence of the electronic specific heat $C_{el}/\gamma_n T$ of LaRu_2P_2 is shown in Figure 1. As shown by open symbol represents the experimental data, we can see two clear discontinuities of specific heat at $T_{c1} = 4.4$ K and $T_{c2} = 4.0$ K, respectively. Each transition temperature vary obeying $H_{c2}(t) = H_{c2}(0)(1-t^2)/(1+t^2)$, where, $t = T/T_{c1}$. This indicates that both discontinuities at T_{c1} and T_{c2} are attributed to superconducting transitions. We tried to analyze our specific heat data by α model [4]. In this model, zero temperature scaled gap $\alpha = \Delta(0)/k_B T_c$ is the only adjustable fitting parameter. In the case of two gaps, the thermodynamic properties of the system are determined as the sum of contributions from the two gaps with individual transition temperatures, that is, $\alpha_1 = \Delta_1(0)/k_B T_{c1}$ and $\alpha_2 = \Delta_2(0)/k_B T_{c2}$ with their respective weights γ_1/γ_n and γ_2/γ_n , where $\gamma_1 + \gamma_2 = \gamma_n$. In

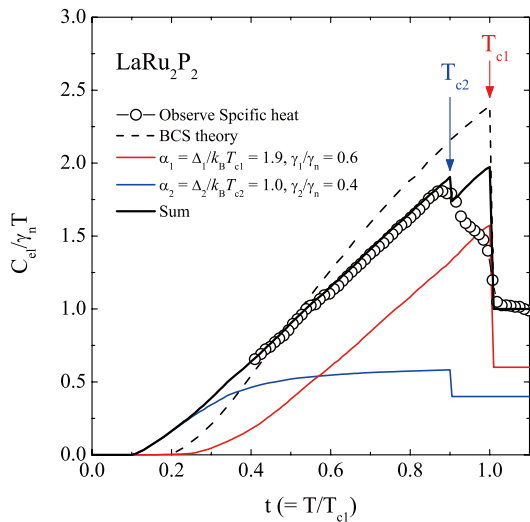


Fig. 1. The normalized superconducting electronic specific heat ($C_{ei}/\gamma_n T$) of LaRu_2P_2 as a function of scaled temperature $t = T/T_{c1}$. The dashed line represents the theoretical curve based on single-band weak-coupling BCS theory. Red and blue solid lines represent the numerically calculated curves of contributions from two gaps and the summation of those contributions are given by black solid line.

Fig.1, numerically calculated $C(T)$ curves are shown together with observed data. Red and blue solid lines represent contributions from each gap to $C(T)$ estimated by adapting $\alpha_1=1.9$ ($\Delta_1(0) = 0.72$ meV) and $\alpha_2 = 1.0$ ($\Delta_2(0) = 0.34$ meV), respectively. Black solid line represents the summation of both contributions and dashed line is the theoretical Curve based on single-band weak-coupling BCS theory with the $\Delta(0)/k_B T_{c1} = 1.76$. The former line well reproduces experimental result over the entire measurement temperature range, indicating that LaRu_2P_2 is the superconductor characterized by two band gaps as well as BaFe_2As_2 based compounds. In addition, N_2 is larger than N_1 , where N_1 and N_2 are DOS at E_F in respective bands. Unfortunately, it is unapparent that how Ru 4d electrons do contribute to these bands at present. To understand the main band occupies the Fermi level, it is required to be studied the detailed electronic structure of LaRu_2P_2 .

References

- [1] Y. Kamihara, T. Watanabe, M. Hirano, and H. Hosono, *J. Am. Chem. Soc.* **130**, 3296 (2008).
- [2] T. Fujiwara, K. Matsubayashi, Y. Uwatoko, and T. Shigeoka, *J. Phys.: Conf. Ser.* **273**, 012112 (2011).
- [3] J. J. Ying, Y. J. Yan, R. H. Liu, X. F. Wang, A. F. Wang, M. Zhang, Z. J. Xiang, and X. H. Chen, *Supercond. Sci. Technol.* **23**, 115009 (2010).
- [4] H. Padamsee, J. E. Neighbor, and A. C. Shiffman, *J. Low Temp. Phys.* **12**, 387 (1973).

Authors

T. Fujiwara^a, H. Sagawa^a, K. Matsubayashi, Y. Uwatoko, and T. Shigeoka^a
^aYamaguchi University

Surface Relaxation of Topological Insulator: Influence on the Electronic Structure

N. Fukui, T. Hirahara, and T. Takahashi

Topological insulators are now being investigated enthusiastically for their peculiar properties which stem from the inverted parity band structure. For example, previous researches found that surface states of a topological insulator form a spin polarized Dirac cone with a linear dispersion.

The electronic structures of topological insulators have been studied extensively, but little has been studied on their surface atomic structure.

Here we report the surface structures of two topological insulators, Bi_2Te_3 and a single bilayer Bi on Bi_2Te_3 (Bi1BL hereafter), by LEED analysis. There was only a slight relaxation on the Bi_2Te_3 surface, showing that the bulk atomic structure is maintained in the surface topmost layers. On the other hand, we found that Bi1BL was strongly distorted from bulk Bi; contracted in the in-plane direction and expanded in the out-of-plane direction. Figs. 1 (a) and (b) are the optimized surface structure of Bi1BL obtained from the LEED analysis. The red solid lines in Fig. 1 (c) are the measured intensity-voltage curves (IV curves) and the blue broken lines are those calculated from the optimized atomic structure. The in-plane lattice constant of the topmost Bi1BL matches to that of Bi_2Te_3 of 4.38\AA which is 3% contracted from the corresponding lattice constant of bulk Bi (4.54\AA) [1]. Note that this contraction does not take place on a Si(111) substrate [2]. In contrast, the intralayer distance of 1.71\AA was expanded by 7% from the bulk value (1.59\AA). The Poisson ratio almost reaches 0.5, the theoretical maximum of an elastic material.

Ab initio calculations revealed the influence of this strong distortion. Fig. 2 shows the band structure of a free standing Bi bilayer with the lattice constants of bulk Bi (a), and that of distorted Bi with the experimentally determined parameters (b). It is found that the energy gap is enlarged from 0.1eV to

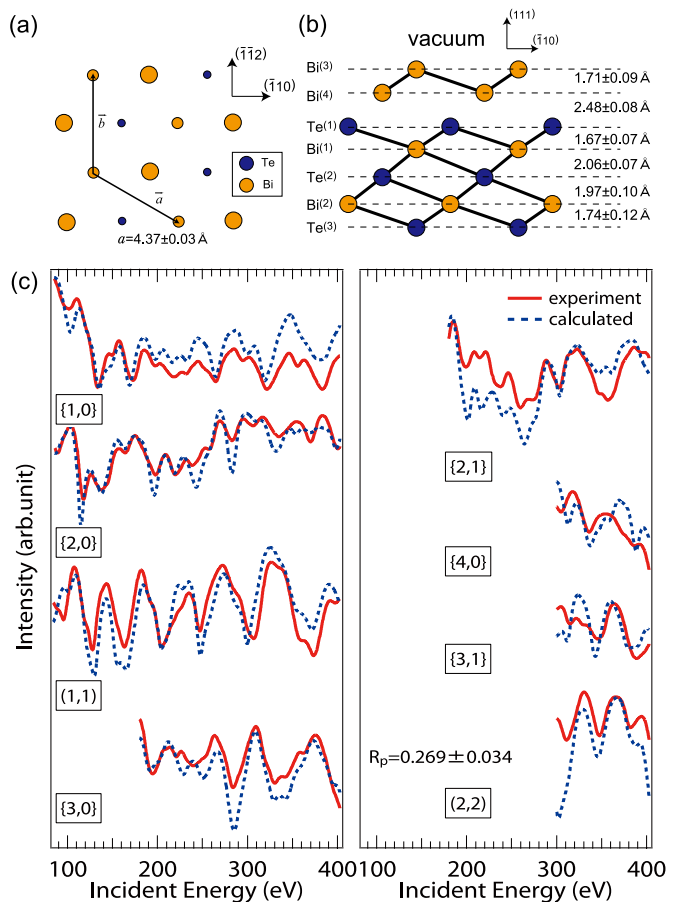


Fig. 1. The top view (a) and the side view (b) of the optimized surface atomic structure of Bi1BL on a Bi_2Te_3 substrate. The orange circles and the blue circles represent the position of Bi atoms and Te atoms, respectively. In (a), the size of a circle indicate the depth of the atom from the topmost layer. (c) The obtained IV curves (red solid lines) and the calculated ones (blue broken lines). R_p is 0.27, where R_p is Pendry's reliable factor and indicates the degree of agreement.

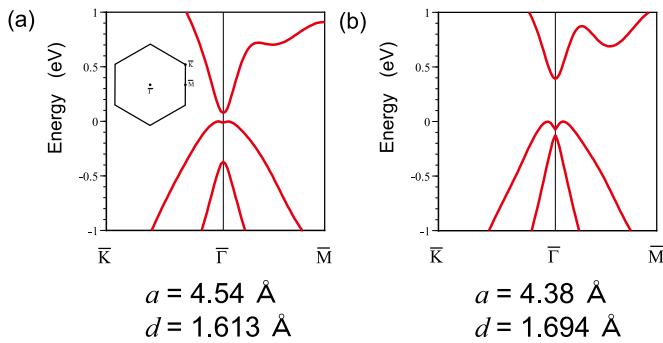


Fig. 2. The band structure of a free standing Bi1BL (*ab initio* calculations) for the lattice constants of bulk Bi (a), and that for Bi which is contracted in-plane and expanded out-of-plane as experimentally determined (b). The inset represents the first Brillouin zone of Bi1BL and the high symmetry points. a is the in-plane lattice constant and d is the out-of-plane lattice constant.

0.4eV when the lattice constants are changed.

In summary, we showed that the surface atomic structure relaxation of Bi1BL has a strong impact on its electronic structure. Changing the in-plane lattice constant can be a means to obtain a topological insulator with a wider band gap.

References

- [1] H. Mönig, J. Sun, Yu. M. Koroteev, G. Bihlmayer, J. Wells, E. V. Chulkov, K. Pohl, and Ph. Hofmann, *Phys. Rev. B* **72**, 085410 (2005).
- [2] T. Nagao, J. T. Sadowski, M. Saito, S. Yaginuma, Y. Fujikawa, T. Kogure, T. Ohno, Y. Hasegawa, S. Hasegawa, and T. Sakurai, *Phys. Rev. Lett.* **93**, 105501 (2004).

Authors

N. Fukui^a, T. Hirahara^a, T. Shirasawa, T. Takahashi, K. Kobayashi^b, and S. Hasegawa^a

^aThe University of Tokyo

^bOchanomizu University

Buckling-induced Direct π -Band Gap Opening in Epitaxial Silicene

R. Friedlein

As the Si counterpart of graphene, “silicene” may be defined as an at least partially sp^2 -hybridized, atom-thick honeycomb layer of Si atoms that possesses π -electronic bands [1]. Astonishing electronic properties, such as the presence of a Dirac cone, are expected to prevail even in its predicted, stable, slightly-buckled form where neighboring Si atoms are displaced out of plane [2,3]. However, different to graphene, because it can be easily buckled, silicene may exist in a variety of lattice constants, atomistic structures and with a varying sp^2/sp^3 ratio.

In a comprehensive study employing a combination of scanning tunneling microscopy (STM), angle-resolved valence band (ARUPS) and core level photoelectron spectroscopy, as well as theoretical calculations, we could 1.) demonstrate the reproducible formation of two-dimensional, epitaxial silicene on single-crystalline $ZrB_2(0001)$ thin film surfaces by segregation of Si atoms from the Si substrate, and 2.) reveal the intimate relationship between the internal structure and the electronic properties of such Si honeycomb layers [1]. Information essential to the understanding of structural details of this silicene layer has been obtained from surface-sensitive Si $2p$ photoelectron spectra that were recorded at the ISSP beamline 18A located at the KEK-PF synchrotron radiation facility (Tsukuba, Japan),

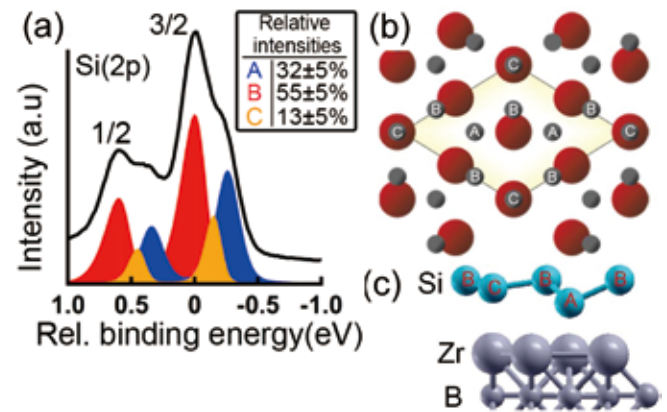


Fig. 1. (a) Surface-sensitive Si $2p$ spectrum recorded at normal emission. Chemical states “A” (blue), “B” (red) and “C” (yellow) have been identified by a peak fitting procedure. (b) Structure model of silicene on $ZrB_2(0001)$. (c) Calculated height profile of silicene on Zr-terminated $ZrB_2(0001)$.

using third-order light (130 eV).

The Si $2p$ spectrum obtained at normal emission, shown in Fig. 1a, indicates the presence of Si atoms in three well-defined chemical environments, labeled “A”, “B” and “C”. Within the error bars, the intensity ratio of 2:3:1 for the three components matches the single in-plane position of a Si honeycomb structure derived from STM images [1] shown in Fig. 1b. As shown in Fig. 2, diffraction of Si $2p$ photoelectrons originating at “A” atoms occurs on “B” along the $[\bar{1}100]$ direction proving the lower position of “A” atoms and atomic-scale buckling. In this structure model, the matching of the $ZrB_2(0001)-(2 \times 2)$ unit cell with that of the Si overlayer provides a $(\sqrt{3} \times \sqrt{3})$ reconstruction of silicene with a yet unpredicted buckling.

ARUPS spectra taken along the $\bar{\Gamma}-\bar{M}-\bar{\Gamma}$ high-symmetry direction (Fig. 2b) show a distinct spectral feature approaches the Fermi level by up to 250 meV at the $\bar{\Gamma}$ point of the repeated Brillouin zone, denoted “ X_2 ” (Fig. 2b). Its upward curvature bears some resemblance to the predicted Dirac cone of π bands of freestanding, non-reconstructed silicene at its K point. It is then clear that the particular reconstruction of the silicene layer leads to a back-folding of π bands into the (now reduced) 1st Brillouin zone and the opening of a direct band gap at the $\bar{\Gamma}$ point.

Bond lengths of 2.266 Å and 2.242 Å calculated for a structure that is in agreement with the experimental results (Fig. 1c) match closely to those predicted for freestanding

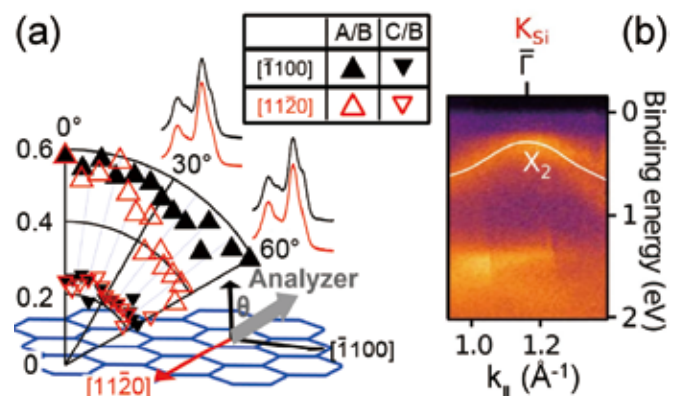


Fig. 2. (a) Intensity ratios A/B and C/B as a function of the polar emission angle ($^\circ$), along the $[110]$ and $[11\bar{2}0]$ directions of the $ZrB_2(0001)$ surface. (b) ARUPS spectra in the vicinity of the $\bar{\Gamma}$ point of the repeated Brillouin zone, taken along the $\bar{\Gamma}-\bar{M}-\bar{\Gamma}$ high-symmetry direction.

honeycomb structures of Si [2,3]. Calculations carried out for a freestanding silicene layer with the same internal structure reveal that the opening of a gap results *primarily* from the particular buckling rather than from the electronic coupling to the substrate. These results imply that the atomistic structure and thus the electronic properties can be changed by the choice of appropriate substrate with selected lattice parameters, something that is (almost) impossible for the rather rigid graphene. The creation of a band gap by the control of the internal structural is likely to be fundamentally relevant for the future use of silicene in devices that perform logical operations.

Experimental help from Dr. K. Yaji and A. Harasawa (ISSP) is highly acknowledged.

References

- [1] A. Fleurence, R. Friedlein, T. Ozaki, H. Kawai, Y. Wang, and Y. Yamada-Takamura, Phys. Rev. Lett. (to be published).
- [2] K. Takeda and K. Shiraiishi, Phys. Rev. B **50**, 14916 (1994).
- [3] S. Cahangirov, M. Topsakal, E. Aktürk, H. Sahin and C. Ciraci, Phys. Rev. Lett. **102**, 236804 (2009).

Authors

R. Friedlein^a, A. Fleurence^a, T. Ozaki^{a,b}, Y. Yamada-Takamura^a
^aSchool of Materials Science, Japan Advanced Institute of Science and Technology (JAIST)
^bResearch Center for Simulation Science, Japan Advanced Institute of Science and Technology (JAIST)

DFT-MD Analysis of TiO₂/Solution Interfaces for Photocatalysis and Solar Cell

Y. Tateyama, M. Sumita, and K. Sodeyama

Though a lot of progress has been made in the development of photocatalysis and solar cell, atomistic mechanisms of the chemical reactions at the solid-liquid interfaces have not been fully understood yet because of the experimental and computational difficulty in analyzing such interfacial processes. In order to solve these problems, we have been studying TiO₂ electrode/liquid interfaces, associated with photocatalysis (PC) and dye-sensitised solar cell (DSC), on the atomic and electronic scales, by use of quantitative theoretical simulations based on the density functional theory (DFT) with supercomputers.

We investigated the TiO₂ anatase (101) and (001) interfaces, a most representative PC system, dipped in bulk water on the atomic scale by DFT molecular dynamics (MD) simulations, in order to elucidate the behaviour of water molecules and hydrogen bond (HB) networks at the interfaces [1]. It is demonstrated that the adsorption manners (molecular or dissociative) of water molecules on the

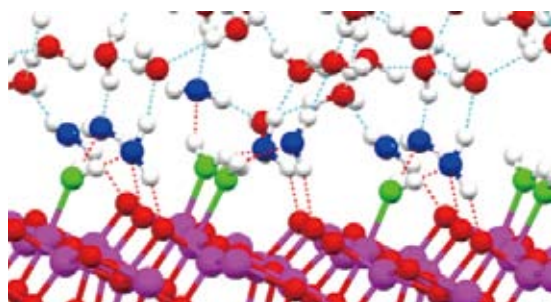


Fig. 1. Equilibrium structure of TiO₂ anatase (101)/ liquid water interfaces. Molecular adsorption of water with strong hydrogen bond is observed. The water coverage is around 0.6.

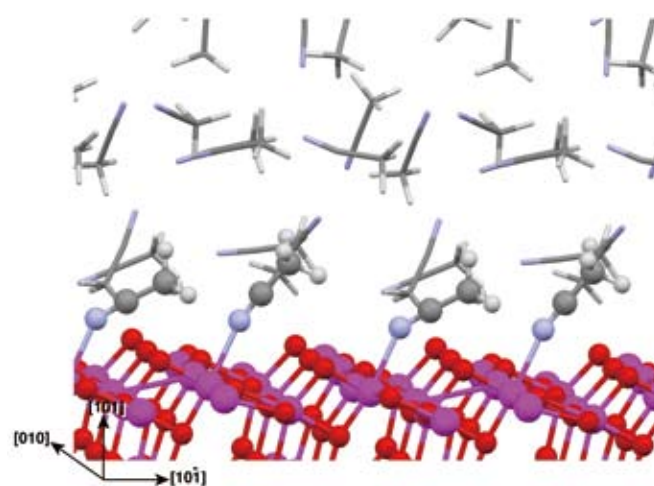


Fig. 2. Equilibrium structure of TiO₂ anatase (101) / liquid MeCN interface for efficient DSCs.

vacuum surfaces still hold in the presence of "bulk" water on the interfaces. On the contrary, novel adsorption structures of interfacial water molecules are found as well. We also show explicit atomistic structures of strong and weak HBs at the TiO₂/H₂O interfaces, which had been proposed experimentally so far. We then suggested a two-layer model for the interfacial water on both surfaces investigated. Our results also give insights into the H₂O or OH adsorption coverage at the interfaces and their hydrophobicity and hydrophilicity. To understand the reaction reactivity, we have recently analyzed the equilibrium electronic states of several TiO₂/H₂O interfaces as well, and found novel microscopic mechanism of the TiO₂ photocatalytic reactions.

We have investigated the DSC interfaces as well. TiO₂ anatase (101) / liquid acetonitrile (MeCN) interfaces and its water contamination effect were examined by DFT-MD simulations [2]. We clarified the characters of MeCN adsorption and the interfacial MeCN under thermal equilibrium. We also found that unusual way of adsorption is the most stable for the contamination water around the TiO₂/MeCN interfaces. The calculated electronic states give an insight into atomistic effect of such water on the dye adsorption and then the durability of DSCs.

We have also examined the adsorption of a Ru N749 dye, so called black dye showing one of the highest conversion efficiency, on the TiO₂ anatase (101) surface [3]. Our calculations suggest that this black dye prefers keeping proton energetically, implying that the TiO₂ surface is rather acidic. Regarding the photoexcitation spectra, our TDDFT calculations reproduce the red shift of the onset compared to that of

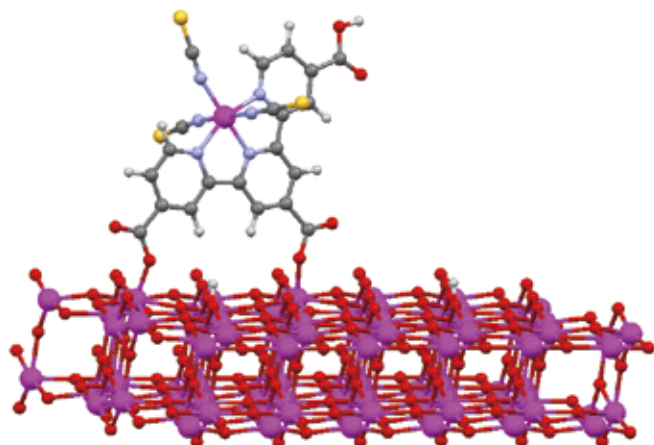


Fig. 3. Schematic picture of black dye adsorption to TiO₂ anatase (101) surface for an efficient DSC.

the most famous N3 dye.

References

- [1] M. Sumita, C. Hu, and Y. Tateyama, *J. Phys. Chem. C* **114**, 18529 (2010).
 [2] M. Sumita, K. Sodeyama, L. Han, and Y. Tateyama, *J. Phys. Chem. C* **115**, 19849 (2011).
 [3] K. Sodeyama, M. Sumita, C. O'Rourke, U. Terranova, A. Islam, L. Han, D. R. Bowler, and Y. Tateyama, *J. Phys. Chem. Lett.* **3**, 472 (2012).

Authors

Y. Tateyama^{a,b,c}, M. Sumita^{a,b}, and K. Sodeyama^{a,b}
^aWPI-MANA, National Institute for Materials Science
^bCREST, Japan Science Technology Agency
^cPRESTO, Japan Science Technology Agency

Enhanced Piezoelectric Properties of Al-substituted Langasite Family Crystals

H. Takeda, T. Hoshina, and T. Tsurumi

$\text{La}_3\text{Ga}_5\text{SiO}_{14}$ (langasite; LGS) family single crystals are the most attractive piezoelectric materials for use at high temperature, because the crystals show no phase transitions up to its melting temperature. Recently, combustion pressure sensors made of the LGS and $\text{La}_3\text{Ta}_{0.5}\text{Ga}_{5.5}\text{O}_{14}$ (LTG) substrates have been developed on a laboratory scale. A low temperature dependence of the piezoelectric properties and a high electric resistivity at high temperature are still necessary to improve in the langasite family crystals for the practical use. From these reasons, we have developed aluminum substituted LGS, $\text{La}_3\text{Nb}_{0.5}\text{Ga}_{5.5}\text{O}_{14}$ (LNG) and LTG crystals.

Figure 1 shows the crystals with three Al-contained compositions, $\text{La}_3\text{Ga}_{4.1}\text{Al}_{0.9}\text{SiO}_{14}$ (LGAS0.9), $\text{La}_3\text{Nb}_{0.5}\text{Ga}_{5.3}\text{Al}_{0.2}\text{O}_{14}$ (LNGA0.2), and $\text{La}_3\text{Ta}_{0.5}\text{Ga}_5\text{Al}_{0.5}\text{O}_{14}$ (LTGA0.5), which were grown by Czochralski technique. All the crystals showed a smooth surface, and were transparent with an orange color. No cracks and inclusions were found inside the grown crystals. Although segregation phenomena should occur during crystal growth due to solid solution crystals, all the crystals showed very small variation in the Al_2O_3 concentration. This means that the chemical compositions of LGAS0.9, LNGA0.2 and LTGA0.5 are very close to congruent melting composition.

Langasite family crystals belong to space group $P321$. There are four kinds of cation sites in the structure. They are composed of a decahedral site and an octahedral one, two kinds of tetrahedral ones. Structure analysis revealed that Al atoms are distributed on octahedral and two tetrahedral sites except for the decahedral site, which is occupied by La.

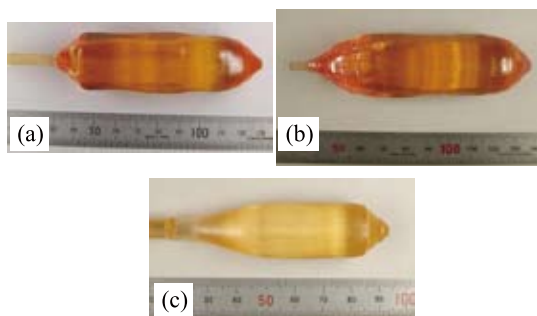
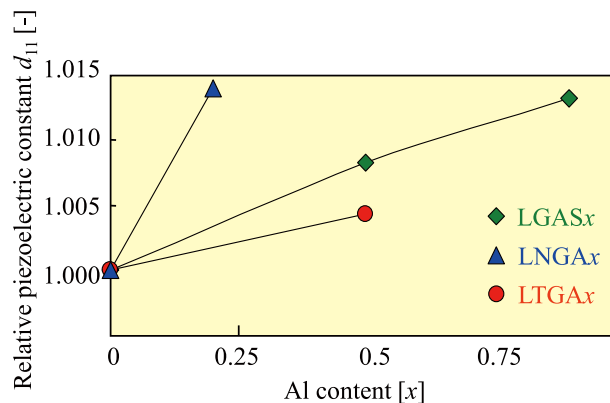


Fig. 1. Aluminium substituted langasite family crystals grown by Czochralski technique. (a) $\text{La}_3\text{Ga}_{4.1}\text{Al}_{0.9}\text{SiO}_{14}$ (LGAS0.9), (b) $\text{La}_3\text{Nb}_{0.5}\text{Ga}_{5.3}\text{Al}_{0.2}\text{O}_{14}$ (LNGA0.2), and (c) $\text{La}_3\text{Ta}_{0.5}\text{Ga}_5\text{Al}_{0.5}\text{O}_{14}$ (LTGA0.5).



Change of piezoelectric d_{11} constant by Al substitution

Fig. 2. Variation of piezoelectric strain d_{11} constants as a function of Al-content for aluminium substituted langasite family crystals.

Isotropic decrement of lattice constants and no systematic change of structural distortion were observed in all the crystal. The decrement of lattice constants proved that Al^{3+} was substituted for Ga^{3+} , because Al has small ionic size and low atomic weight compared with gallium.

Figure 2 shows the changes in the piezoelectric constant d_{11} as a function of x in Al-substituted crystal. With an increase in the Al content, the absolute piezoelectric strain modulus d_{11} increases by about 1.3%, 1.5% and 0.6% for LGAS0.9, LNGA0.2 and LTGA0.5, respectively. This is because elastic compliance constant s_{ij}^E increased with Al content. With increasing Al content, s_{11}^E increased 0.3 to 2.4%. This increment implies that the crystal becomes hard elastically. This should result from shrinkage of the crystal lattice, that is, a decrease of lattice constants a and c , by Al substitution for Ga.

The temperature dependence of the piezoelectric constant d_{11} and electric resistivity ρ were investigated from room temperature to 700°C. Very small influence of Al substitution on temperature dependence in all crystals is observed. The Al substitution hardly affected the thermal behaviour of the piezoelectric properties of the langasite family crystals. The LTGA0.5 crystal shows the smallest variation ($\pm 1\%$) of all the crystals. About the ρ values, the Al-substituted crystals have high ρ values of one order of magnitude, compared with pure crystals at high temperatures. The ρ value is almost satisfied for the required values at 400 °C. The Al substitution is effective way to improve the electric resistivity for the langasite family crystals. Especially, the LTGA0.5 crystal is the most promising candidate for combustion pressure sensor material

References

- [1] H. Takeda, J. Yamaura, T. Hoshina, and T. Tsurumi, *J. Ceram. Soc. Jpn.* **118**, 706 (2010).
 [2] H. Takeda, J. Yamaura, T. Hoshina, and T. Tsurumi, *IOP Conf. Ser.: Mater. Sci. Eng.* **18**, 092020 (2011).

Authors

H. Takeda^a, J. Yamaura^b, T. Hoshina^a, and T. Tsurumi^a
^aTokyo Institute of Technology
^bUniversity of Tokyo

Experimental Realization of Spin-1/2 Triangular-Lattice Heisenberg Antiferromagnet

H. Tanaka and K. Kindo

It is one of the main subjects of condensed matter physics that revealing the ground state of a frustrated quantum magnet. A two-dimensional spin-1/2 Triangular-Lattice Heisenberg Antiferromagnet (TLHAF), which is one of the well-known frustrated quantum magnets, has an ordered ground state of the 120° spin structure. Although the ground state at zero-field is the same as that for the classical spin, the ground state of a small spin TLHAF in a magnetic field cannot be defined with the classical spin model. For example, when an up-up-down spin state in the TLHAF is stabilized in a magnetic field, one-third magnetization plateau must appear in the magnetization process as a quantum effect.

Here, we report the result of magnetization on $\text{Ba}_3\text{CoSb}_2\text{O}_9$ and present verification that this substance is almost the ideal spin-1/2 TLHAF [1]. $\text{Ba}_3\text{CoSb}_2\text{O}_9$ crystallizes in a highly symmetric hexagonal structure $P6_3/$

mmc , and is composed of a single CoO_6 octahedron and a face-sharing Sb_2O_9 double octahedron. Magnetic Co^{2+} ions form regular triangular lattice layers on the ab plane and are separated by the non-magnetic layer of the Sb_2O_9 double octahedron and Ba^{2+} ions. Thus, $\text{Ba}_3\text{CoSb}_2\text{O}_9$ is expected to be categorized as a good two-dimensional magnet.

Figure 1 (a) shows the magnetization process (M) and the derivative magnetization (dM/dH) for $\text{Ba}_3\text{CoSb}_2\text{O}_9$ measured at 1.3 K. The magnetic field was applied up to 53 T and the whole magnetization process on $\text{Ba}_3\text{CoSb}_2\text{O}_9$ was observed. The saturation of the Co^{2+} spin occurs at the saturation field (H_S) of 31.9 T. The increase in magnetization above H_S arises from the large temperature-independent Van Vleck paramagnetism characteristic of Co^{2+} in the octahedral environment [2]. Figure 1 (b) shows the magnetization curves corrected for the Van Vleck paramagnetism. The quantum magnetization plateau is clearly observed at $M_S/3$. Thick dashed and solid lines denote fits by the higher order coupled cluster method [3] and exact diagonalization for a 39-site rhombic cluster [4], respectively. Both theoretical curves include the one-third magnetization plateau but the classical magnetization curves (thin dotted lines) show no one-third magnetization plateau. Although the experimental magnetization curve is smeared around the critical fields due to the finite temperature effect and the small anisotropies of the g factor and the interaction, the agreement between the experimental and theoretical results is excellent. This work verifies recent theory on the magnetization process for the spin-1/2 TLHAF

References

- [1] Y. Shirata, H. Tanaka, A. Matsuo, and K. Kindo, Phys. Rev. Lett. **108**, 057205 (2012).
- [2] M. E. Lines, Phys. Rev. **131**, 546 (1963).
- [3] D. J. J. Farnell, R. Zinke, J. Schulenburg, and J. Richter, J. Phys. Condens.: Matter **21**, 406002 (2009).
- [4] T. Sakai and H. Nakano, Phys. Rev. B **83**, 100405(R) (2011).

Authors

Y. Shirata^a, H. Tanaka^a, A. Matsuo, and K. Kindo
^aTokyo Institute of Technology

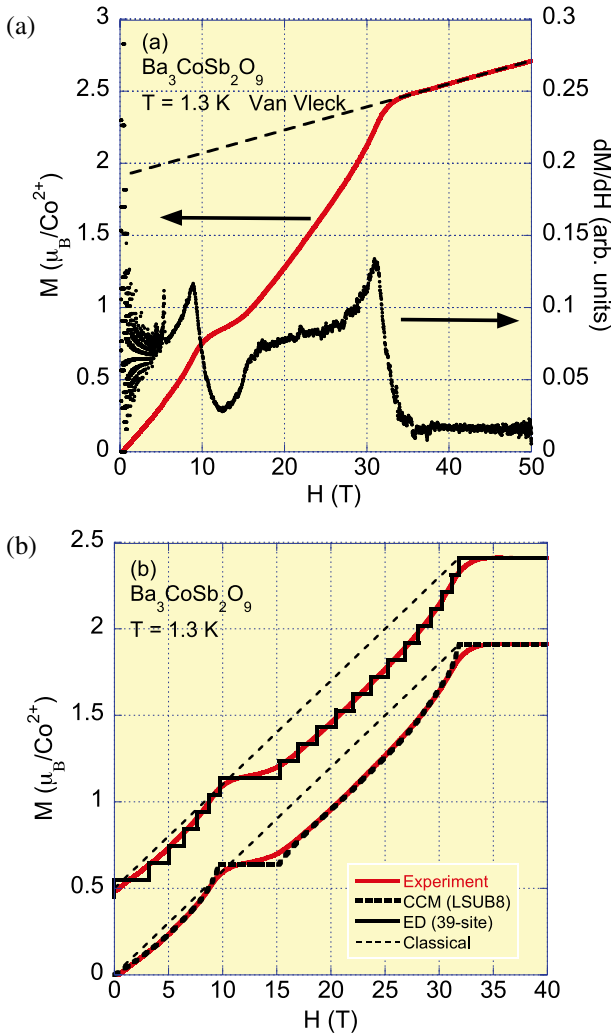


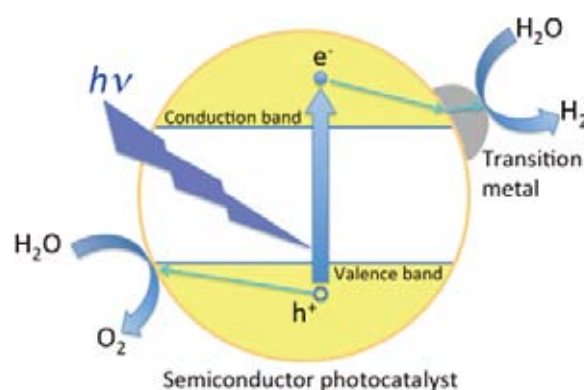
Fig. 1. (a) The magnetization process (M) and the derivative magnetization (dM/dH) for $\text{Ba}_3\text{CoSb}_2\text{O}_9$ at 1.3 K. The saturation field (H_S) is 31.9 T. The increase in magnetization above H_S arises from the large temperature-independent Van Vleck paramagnetism. (b) The magnetization curves corrected for the Van Vleck paramagnetism. The quantum magnetization plateau is clearly observed at $M_S/3$. Thick dashed and solid lines denote fits by the higher order coupled cluster method (CCM) and exact diagonalization (ED) for a 39-site rhombic cluster, respectively. Thin dotted lines show the classical magnetization curves.

ISSP Workshops

Chemistry and Physics of Energy Conversion Materials

November 14-16, 2011
J. Yoshinobu

After the disaster by the Great East Japan Earthquake, we need to seriously consider the effective use of natural energy including solar energy, wind power, geothermal heat etc., where we have to convert these natural energies into more convenient electric power and chemicals using solar cells, catalyst (photocatalyst), thermoelectric devices etc. In the energy conversion processes in such materials, elementary processes at surface and interface play an important role, such as electron-hole pair excitation, charge transfer, charge separation and elementary reactions at a surface/interface. Although materials and devices are different, the concepts may be common. In order to exchange their ideas, the researchers in different fields got together and discussed the physics and chemistry in energy conversion materials including organic solar cell, photocatalyst, electric battery as well as bio-materials, theoretically and experimentally, in this ISSP workshop.



Defects and Topology in Quantum Condensed Systems

January 5-7, 2012

M. Kubota, Y. Okuda, M. Tsubota, M. Oshikawa, and M. Sato

The workshop started by opening address by Prof. Iye, director of ISSP, the university of Tokyo. Participants are from not only classical quantum liquids and solids field with various restricted geometries, but from dilute gas BEC systems and high temperature superconductivity as well as topological superconductors and insulators. Workshop consisted of oral presentations with 20 and 30 minutes length and of poster sessions, for which every presenter had 90 second preview presentation.



Defects and topology used to be the subject related solely to “dislocations, quantized vortices and quantum Hall systems” in the condensed matter physics, but now it is actively studied field covering much wider range of topics, and emphasis is more on the topology in the momentum space. Interesting subject systems include supersolidity of the quantum solid, hcp ^4He , superfluid turbulence in superfluids ^4He and ^3He , as well as in Bose Einstein Condensates (BEC) of neutral atomic gas systems, spontaneous mass flow at the edge of superfluid $^3\text{He-A}$, the intrinsic angular moment of Cooper pairs in a Fermi system as superfluid ^3He and others. Japanese scientists have been making important contributions to understanding these remarkable phenomena. Topological insulators, topological superconductors and Dirac Fermions are new members.

The program and abstracts (text is mostly English, where the table is in Japanese) are given at: <http://www.issp.u-tokyo.ac.jp/public/tanki20120105/>



ISSP Supercomputer: Annual Meeting for Joint Use Activity Report 2011

February 20-21, 2012

N. Kawashima, O. Sugino, H. Noguchi, S. Tsuneyuki, Y. Tomita, H. Watanabe, Y. Noguchi, H. Shiba, and Y. Matsuda

Every year, we hold a workshop for the joint use of the ISSP supercomputers. This year, the meeting was coorganized with the national project "Grand Challenges in Next-Generation Integrated Nanoscience", of which ISSP is the sub-headquarters. During the two days of the meeting, we had 26 oral presentations, and 41 poster presentations, each followed by active discussions. Approximately 80 scientists participated each day. The subjects of the presentations ranged from fundamental aspects of quantum matters to semi-conductor devise, and new energy resources. We invited five distinguished researchers. Masaki Sato (Atmosphere and Ocean Research Institute, U. Tokyo) talked about whole-globe simulation of clouds, and the presentation of Masahiko Machida (Japan Atomic Energy Agency) was on their approach to soil-contamination due to the atomic power plant accidents from the view point of computational condensed matter physics. The other three invited speakers were selected from the users of the ISSP super computers: Kazuhiro Yabana (Tsukuba) talked on the first-principles calculation on optical-pulse propagation, Hiroki Nakano (Hyogo) on exact diagonalization calculation of kagome antiferromagnets, and Hiroshi Shinaoka (AIST) on glassy transition of the frustrated magnets with lattice deformation.



New Scientific Achievements and Future Perspectives at the SPring-8 BL07LSU of the University of Tokyo

February 17, 2012

S. Shin, I. Matsuda, H. Harada, and A. Kakizaki

The workshop was planned to review the present status of the three experimental stations installed in the high-brilliance soft X-ray beamline BL07LSU of the SPring-8 and to discuss the new scientific results obtained there. The workshop was held in the Hongo campus instead of Kashiwa on the occasion of the end of the beamtime of three long-term proposals, which were started 2.5 years ago and carried out by the construction teams. The number of participants was over 40 including invited people from the Ministry of Education and Science, SPring-8 and others. After a brief review of the undulator, beamline and monochromator of BL07LSU, it was reported that the status of each experimental station was already published or accepted for publication as an article in the Rev. Sci. Instrum. In the workshop, the presentations have concerned not only with the recent experimental results but also with the scientific proposals to three apparatuses. As one of the new scientific results obtained from the time-resolved soft X-ray photoemission spectrometer, the carrier dynamics of O/Si(111) surfaces was reported. The high quality of the 3D nano-ESCA apparatus attracted much interests of the application to the analyses of the electronic structures of graphene devices. The soft X-ray emission spectrometer, which achieves a very high energy resolution of 10,000, was adopted to the experiments to investigate the electronic structures of the materials with strongly correlated electron systems, and they revealed many fruitful results already.



Surface States of Topological Insulators

February 23-24, 2012

I. Matsuda, S. Shin, and F. Komori

Three dimensional (3D) topological insulators are unique insulators with metallic surface states, which are caused by nontrivial topology of bulk electronic wavefunctions. These surface states are spin-polarized and show linear dispersion, which result in interesting electronic properties. After the discovery of the first 3D topological insulator, Bi-Sb alloy, several new materials have been developed and intensively studied. In these few years, surface science techniques such as high-resolution angle resolved photoemission spectroscopy (ARPES), spin-and-angle resolved photoemission spectroscopy (SARPES), and scanning tunneling spectroscopy (STS) have been applied to the study of these materials, and novel spin-polarized Dirac electronic states have been clarified.

In this workshop, surface electronic states of topological insulators and related spin-polarized surface states were focused. We had 12 talks on the recent experimental results by ARPES, SARPES and STS, and two talks on the theoretical overview. Discussion on the observations as well as on the details of the experimental methods was the most important part of the workshop.